Progress In Electromagnetics Research C, Vol. 48, 29–35, 2014

Design of a Compact Triple-Band Monopole Planar Antenna for WLAN/WiMAX Applications

Shan Shan Huang*, Jun Li, and Jian Zhong Zhao

Abstract—In this article, a novel miniaturized tri-band monopole antenna for WLAN/WiMAX applications is presented and investigated. The proposed antenna consists of a horizontal H-shaped patch, an L-shaped open end stub, and a deformed inverted T-shaped strip. The patch attached to the 50-Ω feed-line through a matching line can increase the bandwidth of the proposed antenna. The bandwidths under the condition of $|S_{11}| \leq -10$ dB of the proposed antenna are 340 MHz (2.4–2.74 GHz), 340 MHz (3.41–3.75 GHz), and 640 MHz (5.24–5.88 GHz), respectively, indicating this antenna is suitable for WLAN (2.45–2.4835, 5.16–5.35, and 5.725–5.85 GHz) and WiMAX (2.5–2.69, 3.4–3.69, and 5.28–5.85 GHz) applications. The antenna is successfully simulated and measured. Experimental results show that the proposed antenna with compact size of $30 \times 20 \times 0.8\,\text{mm}^3$ has nearly omnidirectional radiation characteristics and stable gains across all the operating bands with a simple structure.

1. INTRODUCTION

In recent years, the demands for using a single antenna covering several wireless communication systems are increasing. In particular, wireless local area network (WLAN) and worldwide interoperability for microwave access (WiMAX) have been developed rapidly. Simple structure, multiple bands, compact size, and low-cost antennas attract worldwide attention. Thus, as one of the key components in wireless communication systems, tri-band planar antenna has received much attention.

Various planar dual-band or tri-band or UWB antennas for WLAN and WiMAX applications have been reported in [1–12]. The antennas proposed in [1–6] are designed for wireless communication systems application and have simple structures. However, they operate at only two bands and cannot cover all the WLAN/WiMAX bands, also, the return losses are too large. The UWB antenna [7–9] can cover all the WLAN/WiMAX bands, but the frequency interference is difficult to avoid for them. In addition, tri-band antennas have been introduced in [10–12]. The proposed antennas using crooked gap and F-shaped [10], folded slot [11], and square-slot with Y-shaped and inverted L-shaped stubs [12] have been investigated. However, these antennas in [10–12] can be used in WLAN/WiMAX systems, but their circuit sizes are $42 \times 40 \times 1.6\,\text{mm}^3$ in [10], $28 \times 30 \times 1.6\,\text{mm}^3$ in [11], and $23 \times 36.5 \times 1.6\,\text{mm}^3$ in [12], which are comparatively large and limit the integration with the wireless communication systems. Also, the structure of the antenna in [11] is comparatively complex.

In this paper, a planar tri-band monopole antenna with simple structure for WLAN and WiMAX applications using a simple horizontal H-shaped strip, an inverted L-shaped stub and a deformed inverted T-shaped strip is introduced. By carefully adjusting the lengths of H-shaped, L-shaped and deformed inverted T-shaped strips, the tri-band antenna centred at 2.5/3.5/5.5 GHz is obtained. The design procedures are given in detail, and the design theory is analyzed and discussed. The proposed tri-band antenna is simulated by a commercial full-wave electromagnetic (EM) simulator ANSYS HFSS and fabricated on a FR-4 substrate. The measured −10 dB bandwidths are 340 MHz (2.4–2.74 GHz),

Received 22 December 2013, Accepted 26 February 2014, Scheduled 4 March 2014
* Corresponding author: Shan Shan Huang (zhiruojingshui@163.com).
The authors are with the School of Electronic and Optical Engineering, Nanjing University of Science and Technology, Nanjing 210094, China.

340 MHz (3.41–3.75 GHz), and 640 MHz (5.24–5.88 GHz), respectively. Moreover, the structure of this antenna is much simple, and the overall circuit size occupies only $30 \times 20 \times 0.8\,\text{mm}^3$ which is very compact. This antenna has nearly omnidirectional radiation characteristics and moderate gains in all the operating bands. Measured results are in good agreement with EM simulation indicates that the proposed antenna is a good candidate for WLAN/WiMAX applications.

2. DESIGN PROCEDURE

Figure 1(a) shows the specific schematic configuration of the proposed tri-band antenna for WLAN and WiMAX applications, which is printed on a $30\times20\times0.8\,\text{mm}^3$ FR-4 substrate with a relative permittivity ε_r of 4.4, a thickness of 0.8 mm and a loss tangent of 0.02. The antenna consists of a horizontal H-shaped patch, an L-shaped open end stub, and a deformed inverted T-shaped strip. In order to reduce the frequency interference between different bands and miniaturize the overall circuit size of the proposed antenna, a matching line with a width of w_1 is connected to the 50-Ω feed line.

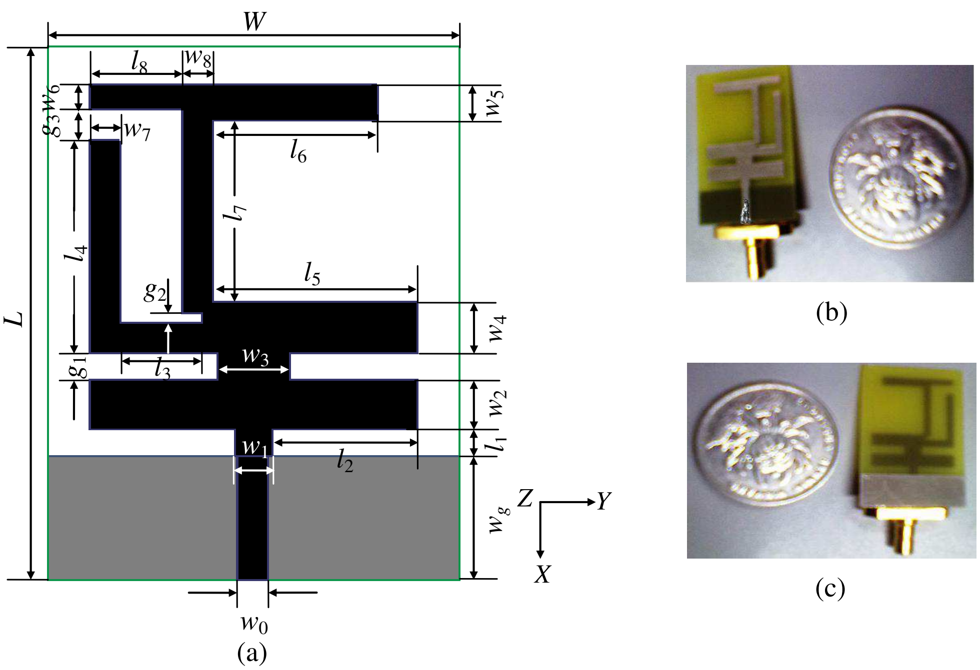

Figure 1. (a) Configuration of the proposed antenna. (b) Top view of the prototype antenna. (c) Bottom view of the prototype antenna.

The three bands of the antenna can be seen as the modification of the single- and dual-band antennas illustrated in the inset of Figure 2. Firstly, the single-band antenna (Antenna 1) is constructed by a horizontal H-shaped patch which is modified from a patch antenna as shown in the inset of Figure 3(a). Secondly, by adding an inverted L-shaped stub to the horizontal H-shaped patch, the dual-band antenna (Antenna 2) is obtained. At last, the tri-band antenna (Antenna 3) is achieved by adding a Z-shaped slot to the L- and H-shaped patch as depicted in Figure 2. Thus, the tri-band antenna centred at about 2.5/3.5/5.5 GHz is obtained. The simulation is performed by the full-wave EM simulator ANSYS HFSS, and the simulated frequency responses are shown in Figure 2. From Figure 2, it is clear that the bandwidths of the proposed tri-band antenna are 2.4–2.7 GHz, 3.4–3.72 GHz, and 5.06–5.85 GHz, whereas the three bands are created by inverted L-shaped stub, inverted T-shaped strip, and H-shaped patch, respectively. It can be observed that, the third resonant frequency increases slightly (from 5.4 GHz to 5.6 GHz), which is possibly due to the coupling inside the inverted L-shaped stub caused by the subtracted Z-shaped slot.

The resonant frequencies of the antenna are determined by the lengths of different resonant sections. The first resonant frequency (centre frequency of the first band f_1) is determined by the resonant section

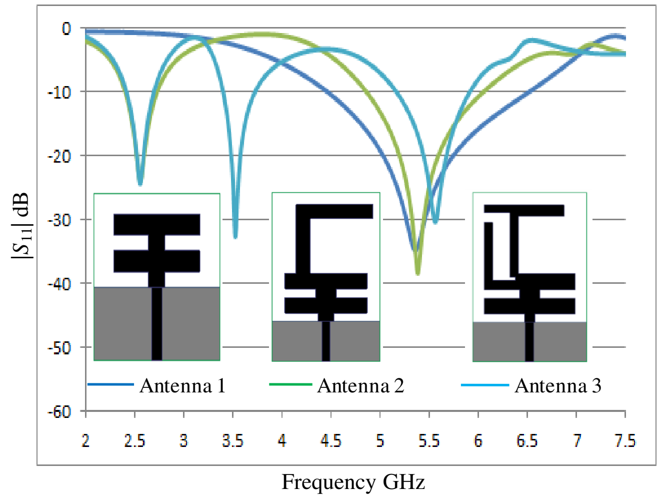

Figure 2. Simulated frequency responses of single-/dual-/tri-band antennas.

with length of $l_{p1} = l_6 + l_7 = 18.2\,\text{mm}$, the second resonant frequency (centre frequency of the second band f_2) is determined by the resonant section with length of $l_{p2} = l_3 + l_4 = 15.9\,\text{mm}$, and the highest frequency (centre frequency of the third band f_3) is determined by the resonant section with length of $l_{p3} = l_1 + l_2 = 8.55\,\text{mm}$. The lengths l_{pi} $(i = 1, 2, 3)$ are obtained as

$$l_{pi} = \frac{\lambda_g}{4} \tag{1}$$

$$\lambda_g = \frac{\lambda_0}{\sqrt{\varepsilon_{eff}}} \tag{2}$$

$$\varepsilon_{eff} = \frac{\varepsilon_r + 1}{2} \tag{3}$$

where l_{pi} is the lengths of resonant sections, λ_g the guided wavelength, λ_0 the wavelength in free space, and ε_{eff} the effective dielectric constant.

In designing the proposed tri-band antenna, the geometry parameters of Antenna 1 in Figure 2 should be determined first. Antenna 1 is mainly constructed by a H-shaped patch which is obtained by subtracting two slots in the fundamental rectangular patch antenna as shown in the inset of Figure 3(a), and its resonant frequency f_3 is determined by the length l_{p3}. The return loss is increased with the help of these two slots, and the configuration and simulated return loss of the patch antenna are depicted in Figure 3(a). Figures 3(b) and (c) illustrate the centre frequencies and bandwidths of Antenna 1 under different g_2 and g_3. From these two plots, one can observe that the centre frequency decreases with the increase of g_2, and increases with the increase of g_3. Once l_{p3}, g_2 and g_3 are fixed, Antenna 1 is designed. After Antenna 1 is obtained, Antenna 2 can be designed by adding an inverted L-shaped stub to the H-shaped patch. This inverted L-shaped stub provides another resonant frequency f_1 which is determined by the length l_{p1} without affecting f_3. The design of the triple-band antenna is based on the above-mentioned sing- and dual-band antenna. By adding a Z-shaped slot to the inverted L-shaped section, the tri-band antenna is obtained. In order to reduce the frequency interferences between different bands, the width of the Z-shaped slot is widened. In comparison with the L-shaped slot, Z-shaped slot can not only reduce the circuit size, but also match the impedance.

Figures 4(a), (b), and (c) plot the simulated return losses with varied l_6, l_4, and l_2, respectively. As can be seen from Figure 4, these three parameters are key parameters determining the resonant frequencies. One can clearly observe that, f_1 decreases as l_6 increases whereas f_2 and f_3 almost unchanged; f_2 decreases when l_4 increases without affecting f_1 and f_3; and f_3 decreases with the increase of l_2 whereas f_1 and f_2 are kept unchanged.

The final design parameters of the proposed tri-band antenna are optimized and tabulated in Table 1.

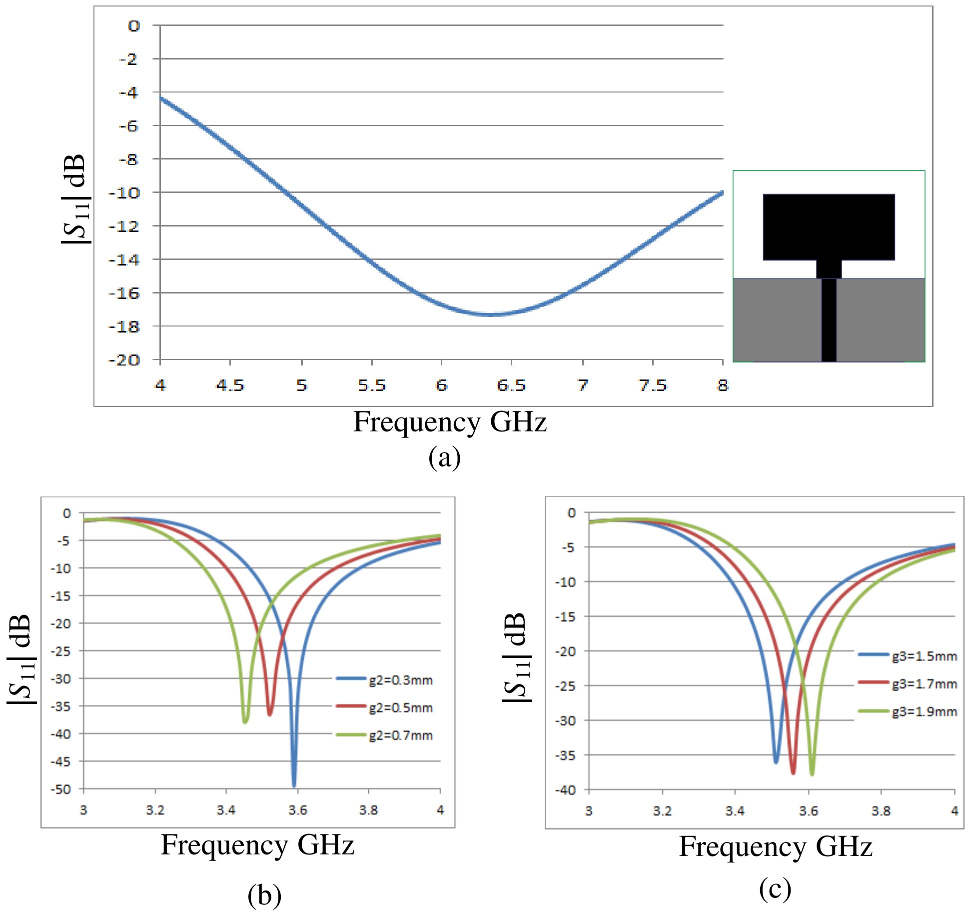

Figure 3. (a) Simulated $|S_{11}|$ of patch antenna. (b) Simulated $|S_{11}|$ of antenna 3 with varied g_2. (c) Simulated $|S_{11}|$ of antenna 3 with varied g_3.

Table 1. Parameters of the proposed antenna.

Parameters	l_1	l_2	l_3	l_4	l_5	l_6	l_7	l_8	w_1	w_2
Values (mm)	1.5	7.1	4	11.9	10	8	10.2	4.5	1.9	2.8
Parameter	w_3	w_4	w_5	w_6	w_7	w_8	W	L	w_g	w_0
Values (mm)	3.5	2.8	2	1.4	1.5	1.5	20	30	7	1.5
Parameters	g_1	g_2	g_3							
Values (mm)	1.5	0.5	1.7							

3. RESULTS AND DISCUSSION

The schematic and photograph of proposed tri-band antenna are shown in Figures 1(a), (b) and (c), and the values of design parameters are tabulated in Table 1. The simulated return loss $|S_{11}|$ of the single-/dual-/tri-band antennas are exhibited in Figure 2, and their configurations are illustrated in the inset of Figure 2. From Figure 2, we can clearly see that the proposed antenna is designed through three steps which have been explained in detail in Section 2. Figure 5 shows the measured and simulated results of the proposed tri-band antenna, and the photograph of the fabricated antenna is in the inset of Figure 5. It was measured by Agilent N5244A vector network analyzer (VNA). From Figure 5, one can clearly observe that the simulated and measured results are in good agreement. The fractional bandwidths

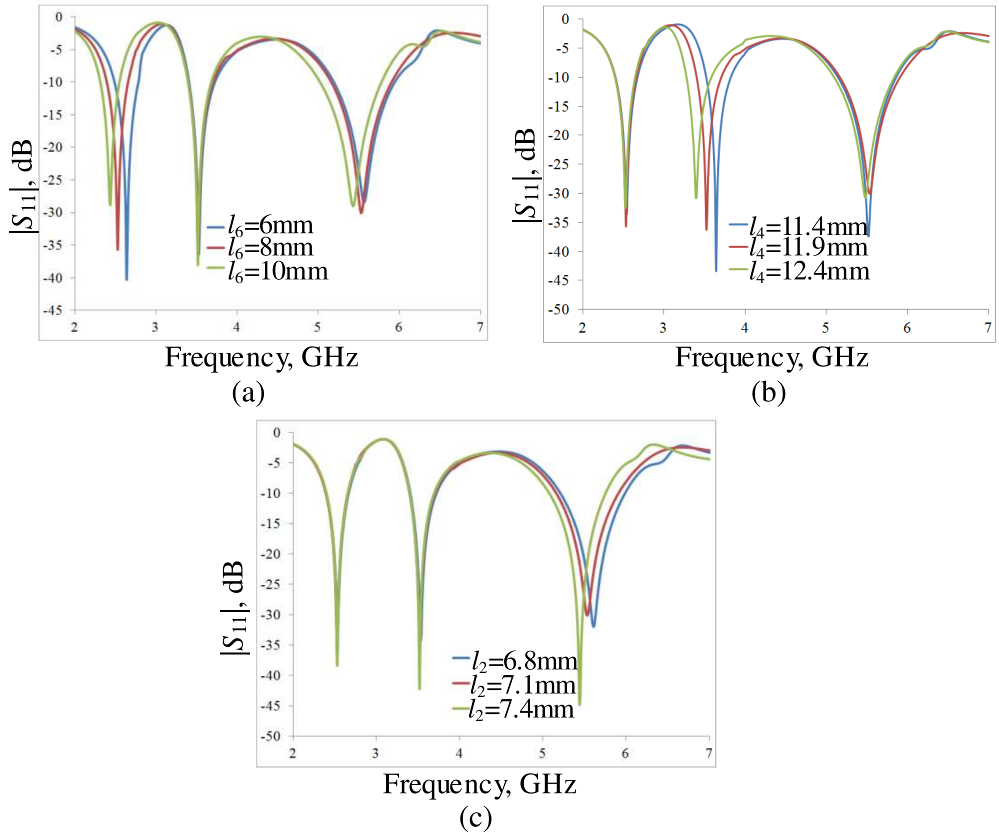

Figure 4. Simulated $|S_{11}|$ of the proposed antenna with varied (a) l_6, (b) l_4, and (c) l_2.

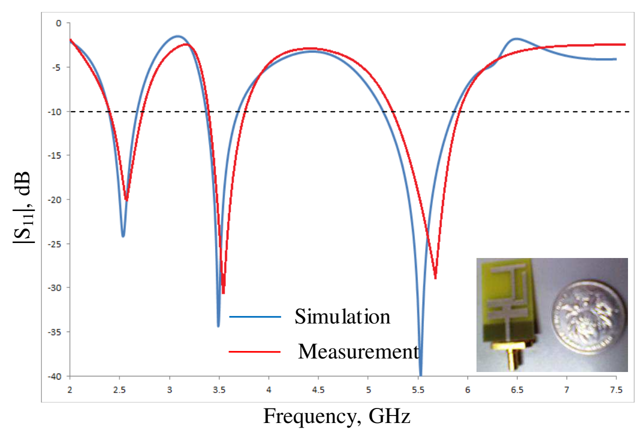

Figure 5. Measured and simulated results of the proposed antenna.

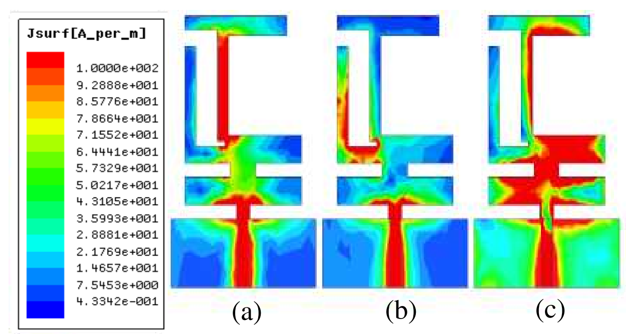

Figure 6. Simulated surface current distribution of the tri-band antenna at (a) 2.5 GHz, (b) 3.5 GHz, and (c) 5.5 GHz.

(FBWs) of the proposed tri-band antenna are 13.23% (2.4–2.74 GHz), 9.5% (3.41–3.75 GHz) and 11.51% (5.24–5.88 GHz), respectively, indicating that this tri-band antenna is totally capable for WLAN and WiMAX applications. Figure 6 exhibits the simulated surface current distribution of the antenna. The maximum current density occurs mainly along the straight line of inverted T-shaped stub at the first resonance (2.5 GHz), as shown in Figure 6(a). The maximum surface current distributes along the inverted L-shaped stub at the second resonance (3.5 GHz), as shown in Figure 6(b). Figure 6(c) reveals

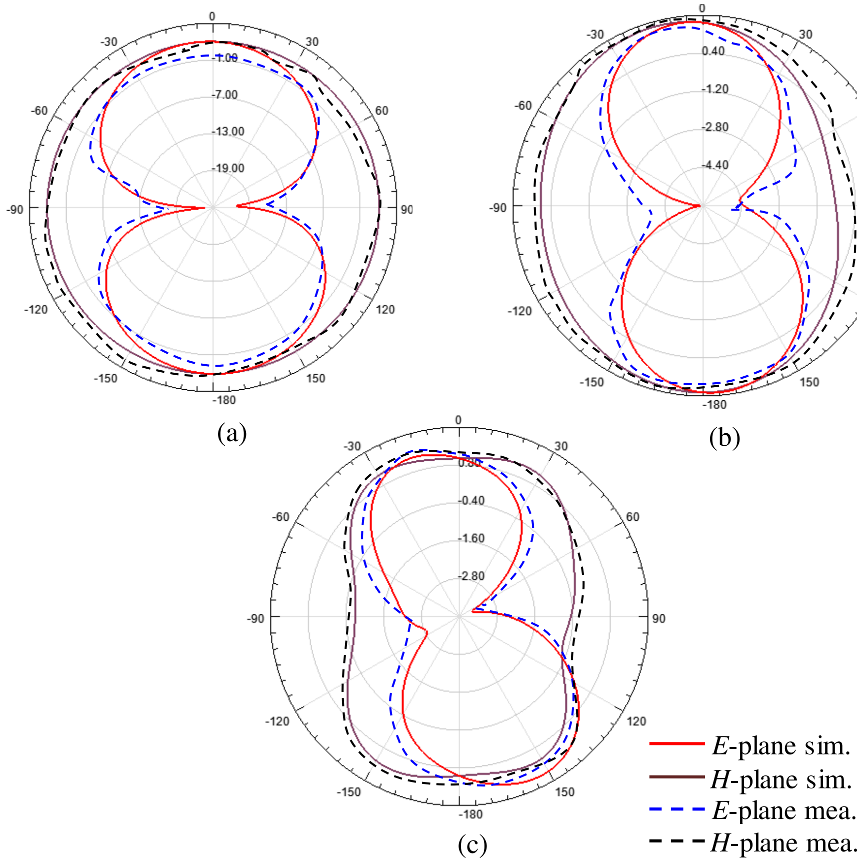

Figure 7. Measured and simulated radiation patterns of the proposed antenna at (a) 2.5 GHz, (b) 3.5 GHz, and (c) 5.5 GHz.

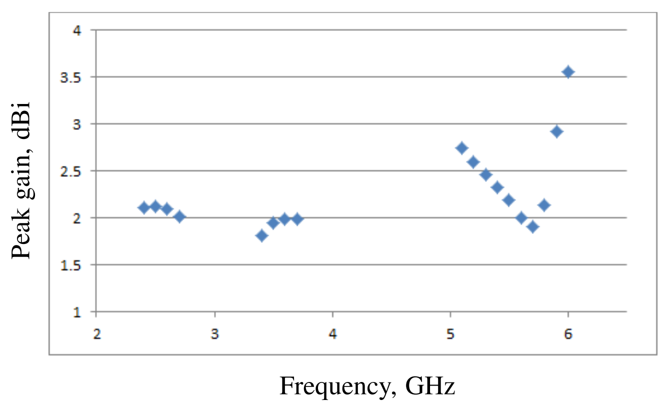

Figure 8. Peak gain of the proposed antenna.

the maximum surface current at 5.5 GHz mostly centralizes at the H-shaped patch. From Figure 6, we can conclude that the first band is determined by the inverted T-shaped, the inverted L-shaped stub influences the second band, and the third band is affected by the H-shaped patch. The measured and simulated far-filed radiation patterns of the tri-band antenna at 2.5/5.5/5.8 GHz are illustrated in Figure 7. Conclusion can be drawn that the far-filed radiation patterns of the proposed antenna are nearly omnidirectional from Figure 7. Figure 8 gives the peak gain of the monopole antenna. The average peak gains for the proposed antenna at three bands are about 2.08/1.93/2.48 dBi, which indicate that the tri-band antenna has stable gains in all the operating bands.

4. CONCLUSION

In this paper, a compact planar tri-band monopole antenna for WLAN/WiMAX applications is presented. The centre frequencies of the proposed antenna is 2.5/3.5/5.5 GHz with FBWs of 13.23/9.5/11.51%. By using a horizontal H-shaped patch, an inverted L-shaped stub, and a deformed inverted T-shaped strip, the tri-band antenna is obtained. The overall circuit size occupies only $30 \times 20 \times 0.8\,\mathrm{mm}^3$ which is very compact. Furthermore, the structure of the proposed antenna is comparatively simple with nearly omnidirectional far-filed radiation patterns and moderate gains. The proposed antenna is very suitable for WLAN/WiMAX wireless communication systems.

REFERENCES

1. Liu, W.-C. and Y.-L. Chen, "Compact strip-monopole antenna for WLAN-band USB dongle application," *Electronics Letters*, Vol. 47, No. 8, 479–480, Apr. 14, 2011.
2. Ojaroudi, N., M. Ojaroudi, and N. Ghadimi, "Dual band-notched small monopole antenna with novel W-shaped conductor backed-plane and novel T-shaped slot for UWB applications," *Microwaves, Antennas & Propagation, IET*, Vol. 7, No. 1, 8–14, Jan. 11, 2013.
3. Hsieh, C. and T. Chiu, "Dual-band antenna design using a dual-feed monopole slot," *Microwaves, Antennas & Propagation, IET*, Vol. 5, No. 12, 1502–1507, Sep. 16, 2011.
4. Wu, C.-M., "Dual-band CPW-fed cross-slot monopole antenna for WLAN operation," *Microwaves, Antennas & Propagation, IET*, Vol. 1, No. 2, 542–546, Apr. 2007.
5. Hua, M. J., P. Wang, Y. Zheng, H. Qin, Y. Liu, S. Yuan, and J. Liao, "Wideband monopole antenna based on CRLH for mobile applications," *Progress In Electromagnetics Research Letters*, Vol. 43, 25–34, 2013.
6. Liu, W.-C. and J.-K. Chen, "Dual-band twin stepped-patch monopole antenna for WLAN application," *Electronics Letters*, Vol. 45, No. 18, 929–931, Aug. 27, 2009.
7. Chacko, B. P., G. Augustin, and T. A. Denidni, "Uniplanar slot antenna for ultrawideband polarization-diversity applications," *IEEE Antennas and Wireless Propagation Letters*, Vol. 12, 88–91, 2013.
8. Lui, W. J., C. H. Cheng, and H. B. Zhu, "Experimental investigation on novel tapered microstrip slot antenna for ultra-wideband applications," *Microwaves, Antennas & Propagation, IET*, Vol. 1, No. 2, 480–487, Apr. 2007.
9. Gautam, A. K., S. Yadav, and B. K. Kanaujia, "A CPW-fed compact UWB microstrip antenna," *IEEE Antennas and Wireless Propagation Letters*, Vol. 12, 151–154, 2013.
10. Yao, J., F.-S. Zhang, X. Q. Jiao, and H. Bai, "Tri-band slotted f-shaped antenna with dual-polarization characteristics for WLAN/wimax applications," *Progress In Electromagnetics Research Letters*, Vol. 40, 181–190, 2013.
11. Zheng, L. and G. Wang, "Design of triple-frequency folded slot antenna for 2.4/3.5/5.2/5.8-GHz WLAN applications," *Progress In Electromagnetics Research Letters*, Vol. 43, 115–123, 2013.
12. Liu, P., Y. Zou, B. Xie, X. Liu, and B. Sun, "Compact CPW-fed tri-band printed antenna with meandering split-ring slot for WLAN/WiMAX applications," *IEEE Antennas and Wireless Propagation Letters*, Vol. 11, 1242–1244, 2012.